34th Annual International Conference of the IEEE EMBS
San Diego, California USA, 28 August - 1 September, 2012

A Feed-Forward Controlled AC-DC Boost Converter for Biomedical Implants

Hao Jiang, Di Lan, Dahsien Lin, Junmin Zhang, Shyshenq Liou, Hamid Shahnasser,
Ming Shen, Michael Harrison and Shuvo Roy

Abstract— **Miniaturization is important to make implants clinic friendly. Wireless power transfer is an essential technology to miniaturize implants by reducing their battery size or completely eliminating their batteries. Traditionally, a pair of inductively-coupled coils operating at radio-frequency (RF) is employed to deliver electrical power wirelessly. In this approach, a rectifier is needed to convert the received RF power to a stable DC one. To achieve high efficiency, the induced voltage of the receiving coil must be much higher than the turn-on voltage of the rectifying diode (which could be an active circuit for low turn-on voltage) [1]. In order to have a high induced voltage, the size of the receiving coil often is significantly larger than rest of the implant. A rotating magnets based wireless power transfer has been demonstrated to deliver the same amount of power at much lower frequency (around 100 Hz) because of the superior magnetic strength produced by rare-earth magnets [2]. Taking the advantage of the low operating frequency, an innovative feed-forward controlled AC to DC boost converter has been demonstrated for the first time to accomplish the following two tasks simultaneously: (1) rectifying the AC power whose amplitude (500 mV) is less than the rectifier's turn-on voltage (1.44 V) and (2) boosting the DC output voltage to a much higher level (5 V). Within a range, the output DC voltage can be selected by the control circuit. The standard deviation of the output DC voltage is less than 2.1% of its mean. The measured load regulation is 0.4 V/kΩ. The estimated conversion efficiency excluding the power consumption of the control circuits reaches 75%. The converter in this paper has the potential to reduce the size of the receiving coil and yet achieve desirable DC output voltage for powering biomedical implants.**

I. Introduction

Biomedical implants have the potential to be widely used in modern medicine. Implants powered by non-rechargeable batteries are largely limited by battery size and life-span. With a recharging mechanism supported by the wireless power transfer technology [3], battery size could be dramatically reduced and life-span could be significantly extended. Therefore, it is essential to have a miniaturized, efficient and reliable wireless power transfer system for biomedical implants.

An inductive coil is used to convert the captured time-varying magnetic flux that is produced by either a RF transmitter [3] or rotating magnets [2] into an AC voltage. Since most implants require a DC power supplier, the induced AC power needs to be rectified to a DC one. The traditional approach is to have a bridge diode rectifier followed by a linear regulator [3]. This approach has two fundamental limitations: (1) The induced voltage at the receiving coil, v_{in}(AC), must be significantly higher than twice of the diode's turn-on voltage, V_{ON}. Otherwise, a significant power loss in the conversion is expected [1][4]. To mitigate this issue, low V_{ON} diodes are currently in development using either the active CMOS circuit [1] or the non-standard semiconductor technology (e.g. Schottky diode [3] or silicon on sapphire [4]); (2) v_{in}(AC) must be higher than the required DC output voltage, V_{out}(DC). To have a high v_{in}, the receiving coil must be large enough (often in cm range [3]), and often is separated from the rest of the implant and placed right under the skin to be close to the transmitting coil [5]. So far, the receiving coil often is the largest component in a miniaturized implant [6].

In order to miniaturize a biomedical implant and place it deep inside of a human body, the power conditioning circuit must be able to convert a low voltage AC power to a high voltage DC power efficiently, especially for charging a battery. To achieve this goal, an innovative feed-forward controlled AC-to-DC boost converter has been demonstrated for the first time. In the wireless power transfer using rotating magnets [2], the induced AC voltage is very slow. Thus, in a small interval, it can be treated as a DC voltage. The circuit is able to convert a 500 mV AC power to 5 V DC. The circuitry architecture and its operating principles are described in Section II. The circuit implementation is depicted in Section III. The measurement results and discussions are reported in Section IV, followed by the conclusions in Section V.

II. Architecture and Operating Principles

Because the induced AC power is low frequency (200 Hz), two small time intervals can be selected when $|v_{in}|$ is high enough. Within this small time interval, the input AC power can be treated as a DC one. Thus, a DC-to-DC boost converter is used to boost the low-voltage input to the high-voltage output, as illustrated in the top half of Fig. 1. First, the switch M_1 is on and the receiving coil shorts itself. During that period, the magnetic energy is stored in the coil with the rising current through the coil L_R. Second, when the switch M_1 is off, the stored magnetic energy in the coil will convert into a voltage source that adds to the input voltage. Thus, the total voltage across the coil is higher than its original input voltage and charge the load during that

Hao Jiang, Di Lan, Junmin Zhang, Shyshenq Liou and Hamid Shahnasser are with School of Engineering, San Francisco State University, San Francisco, California, USA jianghao@sfsu.edu

Ming Shen is with Department of Electronic Systems, Aalborg University, Aalborg, Denmark

Michael Harrison is with Dept. of Surgery, University of California at San Francisco, San Francisco, California, USA

Shuvo Roy is with Dept. of Bioengineering and Therapeutic Sciences, University of California at San Francisco, San Francisco, California, USA

978-1-4577-1787-1/12/$26.00 ©2012 IEEE

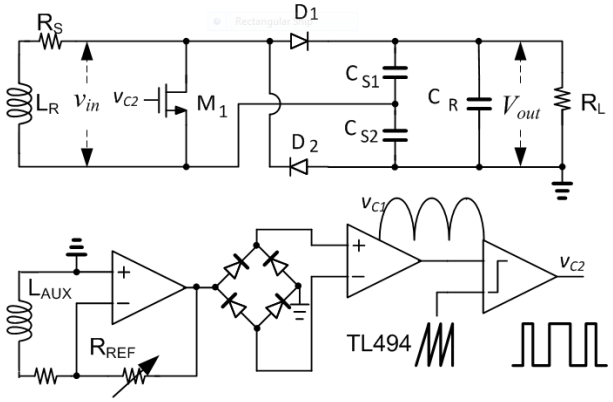

Fig. 1. The simplified circuit diagram of the feed-forward controlled AC to DC boost converter.

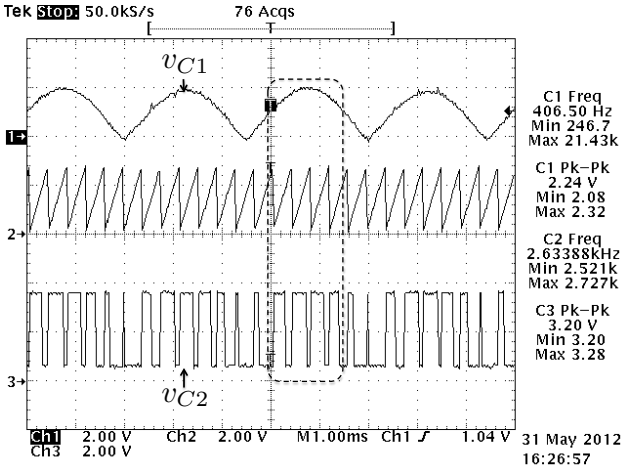

Fig. 2. The measured reference voltage v_{c1} and v_{c2} shown in Fig. 1. v_{c1} is proportional to the absolute value of the voltage from the auxiliary coil. v_{c2} is the gate voltage of the NMOS switch, M_1.

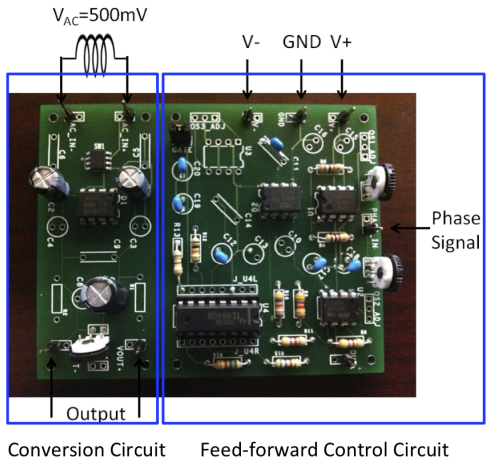

Fig. 3. The photograph of the entire circuits.

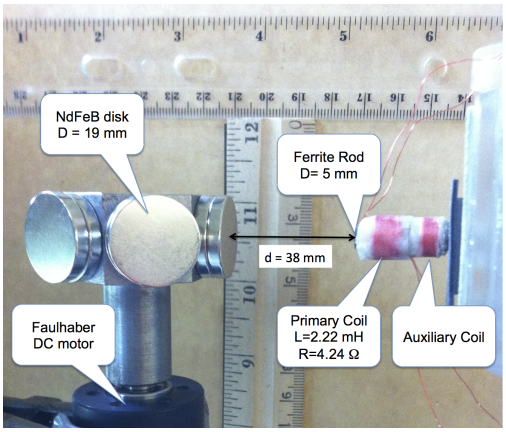

Fig. 4. The photograph of the wireless power transfer using rotating magnets. Both the primary and auxiliary coil are winded on the same ferrite rod with the diameter of 5 mm.

time. At last, the switch M_1 is still off, however, either diode D_1 or D_2 is turned off because the voltage across the coil is finally below the output voltage. The split capacitor topology proposed by [7] (C_{S1} and C_{S2} in Fig. 1) is adopted to boost the input in both positive and negative half cycles. In the positive half cycle, D_2 is off and C_{S1} is being charged. In the negative half cycle, D_1 is off and C_{S2} is being charged. The three capacitors, C_L, C_{S1} and C_{S2}, share energy through charge redistribution [7].

A feed-forward control, instead of traditional feed-back control [7], is used in this paper. The control circuit is illustrated in the bottom half of Fig. 1. In the feed-forward control, the control signal is generated by comparing the voltage signal (v_{c1}) that is proportional to the absolute value of v_{in} (or v_{aux}) to a saw-tooth signal generated by TL494 [8]. v_{c1} is labelled in Fig. 1 and the measured v_{c1} is captured in Fig. 2. The v_{c1} is originated from the induced voltage in the auxiliary coil, v_{aux}. Since the auxiliary coil is next to the primary coil, v_{aux} is able to track both the magnitude and the phase of v_{in} at the primary coil. v_{aux} is first amplified, and then rectified (flipping its negative cycles to positive ones) through a bridge diode rectifier. In this case, the diode's turn-on voltage causes little harm because v_{aux} is amplified before reaching the bridge diode rectifier.

III. Circuit Implementation

Both the boost converter and the feed-forward control circuit are implemented on a printed circuit board (PCB), as shown in Fig. 3. The switch (S_1 in Fig. 1) is a MOSFET that has 25 mΩ turn-on resistance at 4.5 V V_{GS} [9]. The diode (1N4148) (D_1 and D_2 in Fig. 1) is a regular silicon diode with 0.72 V turn-on voltage [10]. The capacitance of the split capacitors (C_{S1} and C_{S2} in Fig. 1) and the load capacitor (C_L in Fig. 1) are 47 μF and 100 μF, respectively.

IV. Measurement Results and Discussions

A. Setup

The measurement setup shown in Fig. 4 is similar to [2]. A rotating magnetic rotor, instead of a coil driven by a RF power source, is used to generate a magnetic field varying at 200 Hz. The disk magnet shown in Fig. 4(a) is made of neodymium iron boron (NdFeB) with 19 mm diameter and

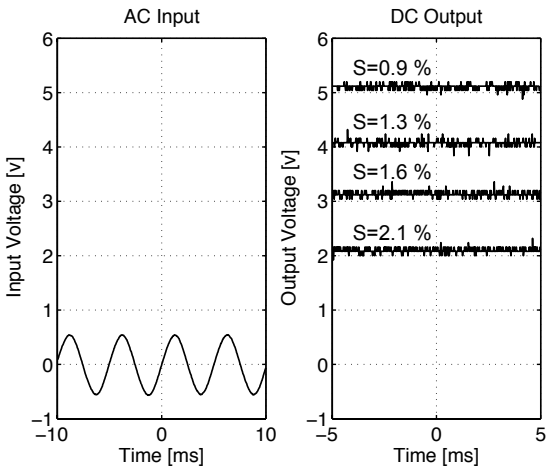

Fig. 5. *Left*: The AC input voltage waveform of the primary receiving coil when it is open. The amplitude and the frequency of the AC input is 500 mV and 200 Hz, respectively *Right*: The output voltage waveform at different $R_{\rm REF}$. S is the ratio of the DC output's standard deviation and mean. R_L used in the measurement is 8.664 kΩ.

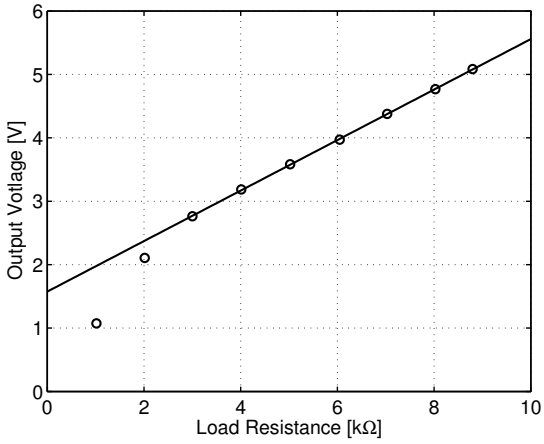

Fig. 6. The output DC voltage is measured versus various load resistance. A linear line is extracted when the load resistance, R_L, ranges from 3 kΩ to 9 kΩ. The slope of the line is 0.4 V/kΩ.

3 mm thickness [11]. The hexagonal rotor driven by a DC motor [12] is made of steel so that all the disk magnets can be attracted to the surface. Each adjacent disk magnet has the opposite polarity. When the rotor rotates $60°$, the receiving coil could experience the maximum variation of the magnetic flux.

Both the primary and auxiliary receiving coils are hand-wound on the same ferrite rod with a diameter of 5 mm [13] to ensure that the induced voltages from both coils are in phase. The diameter and the length of the primary coil is 7 mm and 5 mm, respectively. The inductance and the resistance of the primary receiving coil is 2.22 mH and 4.24 Ω, respectively. The distance from the surface of the magnet to the coil is 38 mm. The induced open-circuit voltage from the primary coil is 500 mV at 200 Hz, as shown in Fig. 5.

B. Output Voltage

An important advantage of this boost converter is that it is able to generate various output DC voltages. Thus, the same converter is able to support various applications. Although there are many charging-discharging pulses in one half cycle, as illustrated in Fig. 1, only the pulses close to the peak charge the load. The duration of the charging time determines the receiving coil's maximum voltage, consequently, the output DC voltage level. Since the charging time can be dynamically controlled by v_{C2} in Fig. 3, the output DC voltage can be effectively set by $R_{\rm REF}$.

In the experiment, the open-circuit AC voltage of the primary coil is kept at 500 mV at the input, as shown in Fig. 5. The load resistance R_L is fixed to 8.664 kΩ. The output voltage is plotted versus time with different $R_{\rm REF}$. Using the particular coil described above, the output DC voltage is able to reach 5 V, which is enough to charge a lithium-ion battery [3]. The stability of the DC output, S, which is measured by the ratio of the standard deviation and its mean, reaches 0.9% at 5 V. By changing $R_{\rm REF}$, the DC output voltage can be tuned to $\sim$ 2.0, 3.0, 4.0 and 5.0 V, as shown in Fig. 5. The measured stability S is less than 2.1% among all these DC output levels.

C. Load Regulation

The load regulation is a measure of the converter's ability to maintain a constant output voltage as a power source despite changes in load.

In the experiment, the output DC voltage is measured when the load resistance, R_L, varies from 1.017 kΩ to 8.797 kΩ. $R_{\rm REF}$ is a constant, so that the DC output voltage is 5 V with 8.664 kΩ R_L. The output DC voltage is plotted versus the load resistance in Fig. 6. The measurement results indicate there is a linear relationship between the output DC voltage and R_L when R_L is in the range from 3 kΩ to 9 kΩ. A linear fit is carried out in this region and the line is plotted in Fig. 6. The load regulation in the region can be described by the slope of the line, which is 0.4 V/kΩ.

D. Efficiency

For biomedical implants, the efficiency of this boost converter is an important figure-of-merit. A highly-efficient power conditioning circuit not only saves the hard-to-get power but also reduces heat dissipation, which is detrimental for clinical applications.

The efficiency of the boost converter, η, is defined as the ratio of the output power P_{out} and the input power P_{in}. In a simple DC-to-DC boost converter, the efficiency is a function of the voltage conversion ratio as well as the value of dissipative circuit components [14]. In this AC-to-DC boost converter, the efficiency, η, is not a constant over time, because the input voltage and the voltage conversion ratio are not constants. Thus, the time averaged efficiency $\overline{\eta}$ is used here.

In the experiment, the output power can be easily calculated by the output DC voltage across the load resistor R_L as $P_{out} = V_L^2/R_L$. However, the input power is hard to measure because both the input voltage and current are

TABLE I

THE DC OUTPUT VOLTAGE WITH DIFFERENT PRIMARY COIL RESISTANCE R_S. THE OPEN-CIRCUIT VOLTAGE OF ALL THREE COILS ARE KEPT AT 500 MV

	R_S [Ω]	P_{av} [mW]	V_{out} [V]	P_{out} [mW]
Coil 1	4.24	7.370	5.083	2.982
Coil 2	5.38	5.809	4.549	2.388
Coil 3	1.35	23.148	8.257	7.889

strongly altered by the switching. A circuit simulator, LTspice from Linear Technology Corp. (Milpitas CA) [15], is used to estimate the averaged input power. The simulation uses models provided by components vendors. The simulated output voltage on a 8.664 kΩ load is 5.19 V (P_{out}= 2.93 mW), while the measured output voltage is 5.083 V (P_{out} = 2.983 mW). Since the simulated output is close to the measured output, the same simulation is employed to estimate the input power. The input power, which is time-averaged, is estimated as $\overline{P_{in}} = \frac{1}{T}\int_0^T v_{in}(t) \cdot i_{in}(t)\ \mathrm{d}t$. Based on the simulated time-averaged input power and the measured output power, the time averaged efficiency is 75%.

E. Coil Resistance

The resistance of the primary coil, R_S shown in Fig. 1, also has profound impact on the performance of the boost converter. R_S could alter the maximum available power inside the primary coil via $P_{av} = \frac{1}{2}\frac{(v_{in}/2)^2}{R_S}$, as well as the power delivered to the converter.

In the experiment, three primary coils with different R_S are wound. By adjusting the distance between the primary coil and the rotating magnets, the open-circuit voltage of all three coils are kept at 500 mV. R_L is 8.664 kΩ. The DC output voltage V_{out} and output power P_{out} are listed in Table I. With the same open-circuit voltage, the coil with smaller resistance possesses more power. However, although it is able to deliver more power to the DC output, its conversion efficiency is not optimal.

V. CONCLUSIONS

In this paper, a feed-forward controlled AC to DC boost converter has been demonstrated for biomedical implants for the first time. This method takes the advantage of the low frequency wireless power transfer, so that the induced AC power can be treated like a DC one over a small time interval. With the amplitude of the harvested AC power as low as 500 mV, this innovative power conditioning circuit is able to convert it to more than 5 V in DC, whereas a traditional bridge diode rectifier will fail. The converter shown in the paper is able to generate various stable DC outputs at high efficiency. The feed-forward control effectively reduces the switching frequency, and consequently, the power for switching. This technology has the potential to significantly miniaturize the coil size used for wireless power transfer and place the coil deep inside of a human body. Since the DC output can reach 5V, this technology will be particularly suited for charging lithium-ion batteries.

ACKNOWLEDGMENT

The authors would like to thank Mr. Philip Frances and Mr. Thomas Franco for their machining support. They are both affiliated with San Francisco State University. The project is partially supported by the Pediatric Device Consortium at the University of California, San Francisco, an FDA grant program (award No. 5P50FD003793-02), the NASA Science and Technoloy Inititive (NSTI) grant and the San Francisco State University Small Research Grant.

REFERENCES

[1] H. M. Lee and M. Ghovanloo, "An integrated power-efficient active rectifier with offset-controlled high speed comparators for inductively powered applications," *IEEE Trans. Biomed. Circuits Syst.*, vol. 58, no. 8, pp. 1749–1760, 2011.

[2] H. Jiang, J. Zhang, S. Liou, R. Fechter, S. Hirose, M. Harrison, and S. Roy, "A high-power versatile wireless power transfer for biomedical implants," in *Annual International Conference of the IEEE Engineering in Medicine and Biology Society (EMBC)*, 2010, pp. 6437–6440.

[3] P. Li and R. Bashirullah, "A wireless power interface for rechargeable battery operated medical implants," *IEEE Trans. on Circuits Syst. II*, vol. 54, no. 10, pp. 912–916, Oct. 2007.

[4] P. T. Theilmann, C. D. Presti, D. Kelly, and P. M. Asbeck, "Near zero turn-on voltage high-efficiency UHF RFID rectifier in silicon-on-sapphire CMOS," in *IEEE RFIC Symposium*, 2010, pp. 105–108.

[5] E. Okamoto, Y. Yamamoto, Y. Akasaka, T. Motomura, Y. Mitamura, and Y. Nosé, "A new transcutaneous energy transmission system with hybrid energy coils for driving an implantable biventricular assist device," *Artificial Organs*, vol. 33, no. 8, pp. 622–626, 2009.

[6] Y. T. Liao, H. Yao, A. Lingley, B. Parviz, and B. Otis, "A 3-uw CMOS glucose sensor for wireless contact-lens tear glucose monitoring," *IEEE J. Solid-State Circuits*, vol. 47, no. 1, pp. 335–344, Jan. 2012.

[7] R. Dayal, S. Dwari, and L. Parsa, "Design and implementation of a direct AC-DC boost converter for low-voltage energy harvesting," *IEEE. Trans. Ind. Electron.*, vol. 58, no. 6, pp. 2387 –2396, June 2011.

[8] TL494, Texas Instrument. http://www.ti.com/product/tl494.

[9] Vishay Siliconix. http://www.vishay.com/docs/71107/si4426dy.pdf.

[10] NXP. http://www.nxp.com/documents/data_sheet/1N4148_1N4448.pdf.

[11] Supermagnetman. http://www.supermagnetman.net.

[12] Faulhaber Group. http://www.faulhaber.com/.

[13] Ferroxcube. http://www.newark.com/ferroxcube/rod5-20-4b1/ferrite-rod-20x5mm/dp/63R5828.

[14] R. W. Erickson and D. Maksimovic, *Fundamentals of Power Electronics*, 2nd ed. Springer Science+Business Media, LLC, 2004.

[15] LT Spice User Manual. http://ltspice.linear.com/software/scad3.pdf.